Supporting Information

Sources of Particulate Matter in the Athabasca Oil Sands Region: Investigation through a Comparison of Trace Element Measurement Methodologies

Catherine Phillips-Smith[1], Cheol-Heon Jeong[1], Robert M. Healy[2], Ewa Dabek-Zlotorzynska[3], Valbona Celo[3], Jeffrey R. Brook[4], Greg Evans[1]

[1] Southern Ontario Centre for Atmospheric Aerosol Research, University of Toronto, Toronto, Ontario, Canada
[2] Analysis and Air Quality Section, Air Quality Research Division, Environment and Climate Change Canada, 335 River Road, Ontario, Canada
[3] Analysis and Air Quality Section, Air Quality Research Division, Environment and Climate Change Canada, 335 River Road, Ottawa, Ontario, Canada
[4] Air Quality Processes Research Section, Air Quality Research Division, Environment and Climate Change Canada, 4905 Dufferin Street, Toronto, Ontario, Canada

Correspondence to: Greg Evans (greg.evans@utoronto.ca)

S.1 Quality Control and Analysis

The Xact incorporates several Quality Assurance and Quality Control measures. With each measurement the instrument takes, it simultaneously measures the concentration of a Pd rod that is located within the instrument to ensure measurement stability (Batelle, 2012). Additionally, every day at midnight, the instrument completes several tests. In one of these tests, the Xact measured the concentrations of metals located within an upscale rod made of Pd, Pb, Cr, and Cd. The three metals, Pb, Cr, and Cd, in the upscale rod represent each energy level the instrument (Batelle, 2012). When the instrument is operating under normal conditions, these measurements are constant with each test. This feature was invaluable during the August, 2013 campaign when there was a drop in the internal Pd measurement values between August 25 and September 2, 2013. As this had the potential to alter the measured metal concentrations, the changing Pd upscale value was linearly regressed against the upscale values of Cr, Pb, and Cd, which were found to have slopes of 0.63, 8, and 3.3, respectively (Figure S1). These relationships were assumed to be the same for all metals within that energy level, and measurements made August 25 to September 2 were then adjusted assuming a constant ratio between the upscale metal concentration and the various metals within its energy level. To validate this assumption, a linear comparison of the sulphur (S) data before, as well as both the raw and corrected S data during the incident was

compared to the collection-efficiency corrected $PM_{1.0}$ SO_4 data measured by a soot particle aerosol mass spectrometer SP-AMS (Willis et al., 2014); the AMS sulphate was divided by three to determine the equivalent sulphur mass. Prior to August 25 the slope of the line was 2.75 (Figure S2); a slope greater than 1.0 was expected given that $PM_{2.5}$ and $PM_{1.0}$ mass values were being compared. However, the slope of 2.75 was greater than that expected due to the difference in size cutpoints alone. For example, comparison of the ambient ion monitor ion chromatograph's (AIM-IC) $PM_{2.5}$ to the AMS's $PM_{1.0}$ data yielded a slope of 1.66 (Figure S3a), which suggested that there is 66% more sulphate in $PM_{2.5}$ than in $PM_{1.0}$. The difference in the slopes of 2.75 vs. 1.66 implied that the Xact might be measuring additional sulphur that was not in the form of sulphate. However, comparison of the Xact sulphur with the AIM-IC or $PM_{2.5}$ filter data, as described below, indicated that the Xact sulphur values were on average only 40% too high. The additional 17% divergence with the AMS data could not be resolved. As described below, the accuracy of most other metal(oid)s determined by the Xact was much better than that for sulphur.

Correcting the Xact S data for Aug 25-Sept 2 based on the concentration-dependent equations seen in Figure S1 raised the r^2 value from 0.92 to 0.98, and changed the slope of the line from 1.60 to 3.57 (Figure S2). The large change in the slope of the line from 2.75 before August 25 to 3.57 could have been due to an increase in sulphate size distribution. It is more likely that the data after August 25, 2013 may have been over corrected by up to 20%. This represented 35% of the total Xact data used in the PMF analysis.

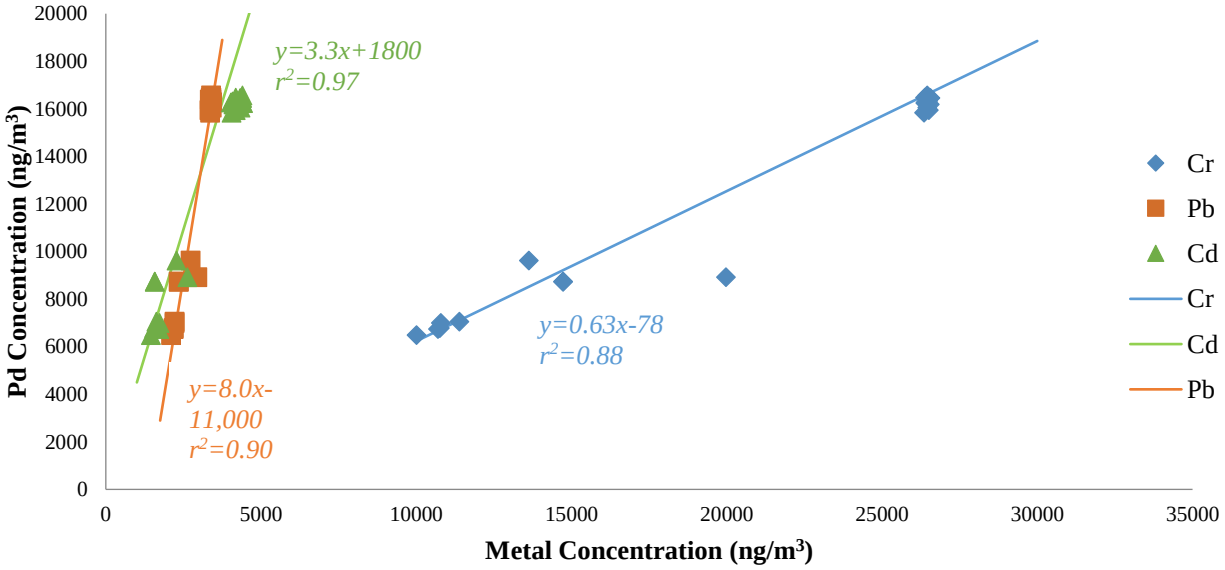

Figure S1. Comparison of Pd rod concentration to the three measured upscale metals: Cr, Cd, and Pb that were measured throughout the intensive campaign.

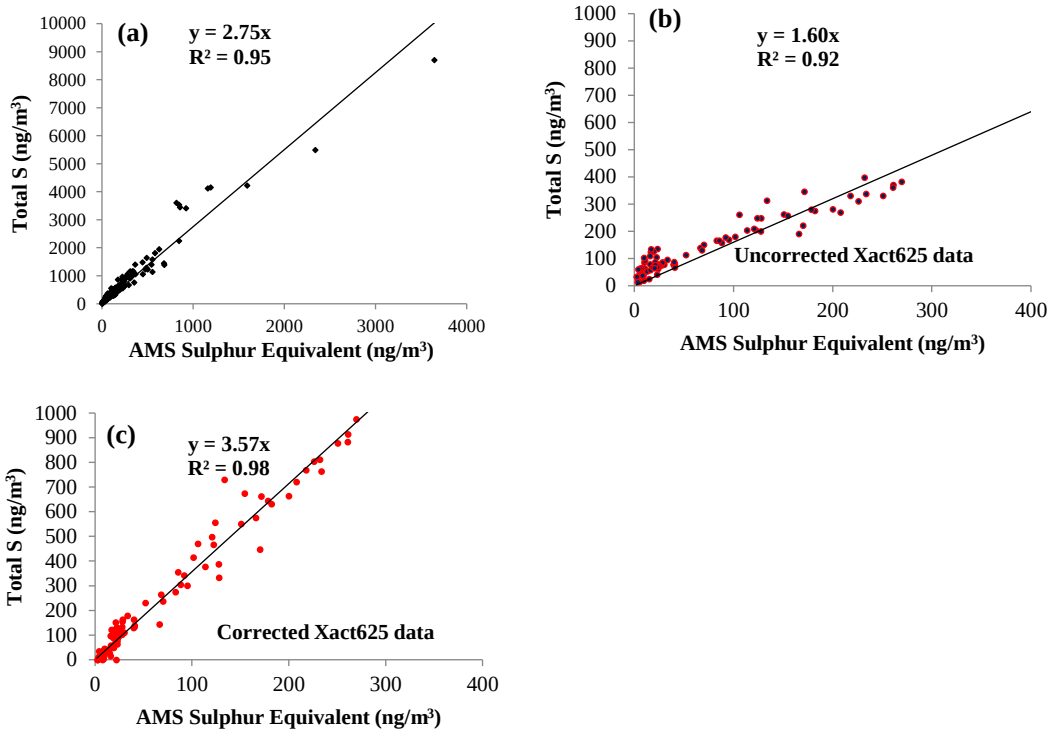

Figure S2. a) Comparison of SP-AMS sulphur equivalent to Xact S before Aug. 25, 2013, b) comparison of SP-AMS sulphur equivalent to raw Xact S data after Aug. 25, 2013, and c) comparison of SP-AMS sulphur equivalent to corrected Xact S data after Aug. 25, 2013. All the SP-AMS sulphate values were divided by three to determine equivalent sulphur mass values.

A comparison of the 1-hr instrumentation data against the coincident 23 -hr filter data was conducted to ensure the data measured with the Xact was equivalent to that measured with the filters. The 1-hr data was averaged between 8:30 am and 7:30 am to correspond with the period during which the filter sample was taken. Any averaged values that were below the detection limit (DL), or calculated using data more than 50% of which were below the DL, were removed. The data was then divided into three groups: low, medium, and high concentrations. Low-concentration metals, those with average values <10 ng/m^3 (Figure S3b), exhibited excellent agreement, with a linear slope of 1.03 and an r^2 value of 0.95 (Xact to Filter data). This represented 63% of the metals measured by the Xact used in the PMF analysis. The medium-concentration metals, those with averages between 10 ng/m^3 and 50 ng/m^3 (Figure S3c), had a slope of 0.77 and an r^2 of 0.99, while the high-concentration elements, with averages above 50 ng/m^3, such as sulphur, had a slope of 1.43 and an r^2 of 0.99 (Figure 3d). The sulphur data was also linearly regressed against the SO_4 data measured with an ambient ion monitor ion chromatograph (AIM-IC), which was divided by three to estimate the S equivalent concentration (Markovic et al., 2012). The result was a line with

a slope of 1.42 and an r^2 of 0.84 (Figure 3), this further indicated the likely presence of a 40% bias in the Xact sulphur measurements.

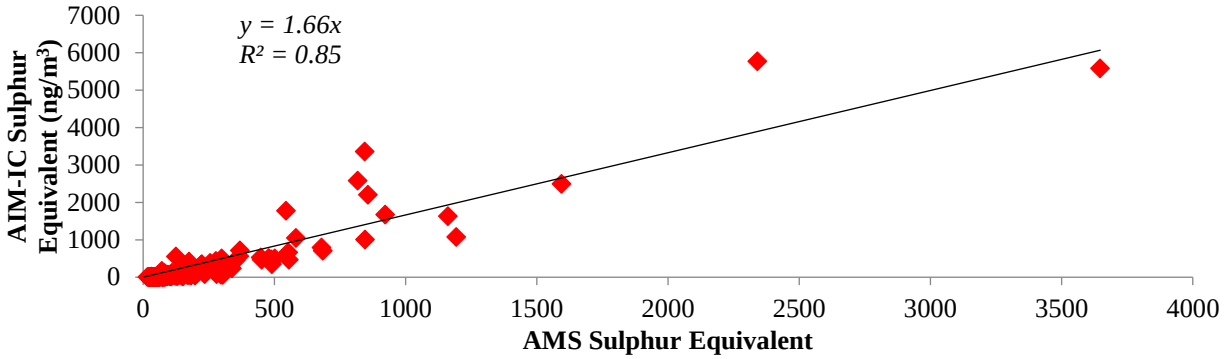

Figure S3a. $PM_{2.5}$ concentrations measured by the AIM-IC to $PM_{1.0}$ concentrations measured by the AMS comparison S before Aug. 25, 2013.

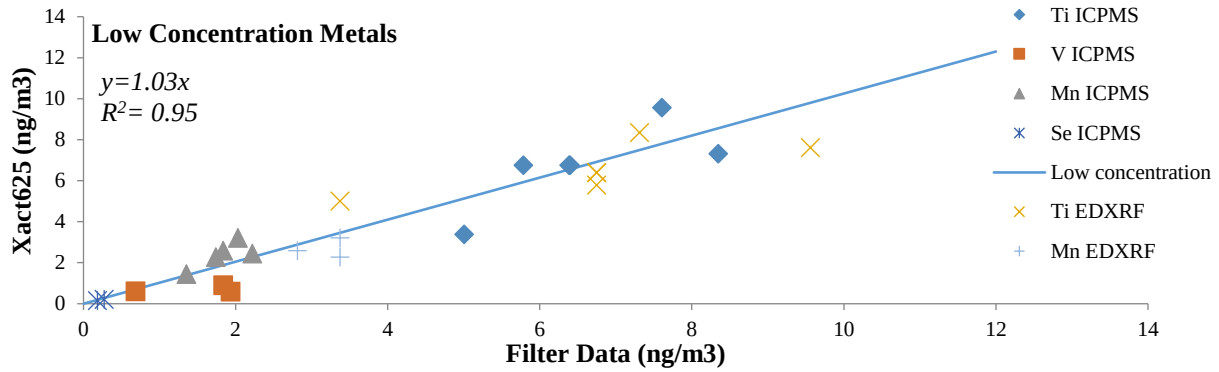

Figure S3b. Filter-Xact comparison for metals with average concentrations <10 ng/m^3.

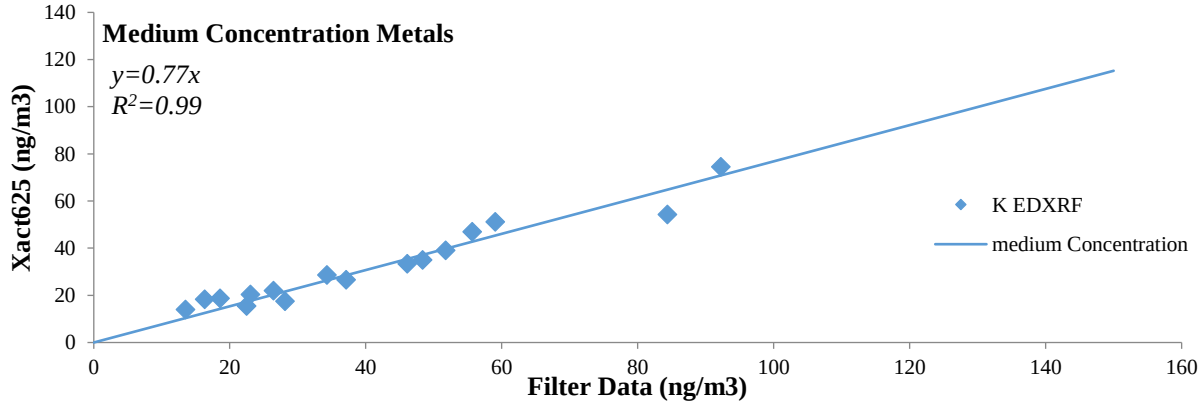

Figure S3c. Filter-Xact comparison for metals with average concentrations >10 ng/m^3 and <50ng/m^3.

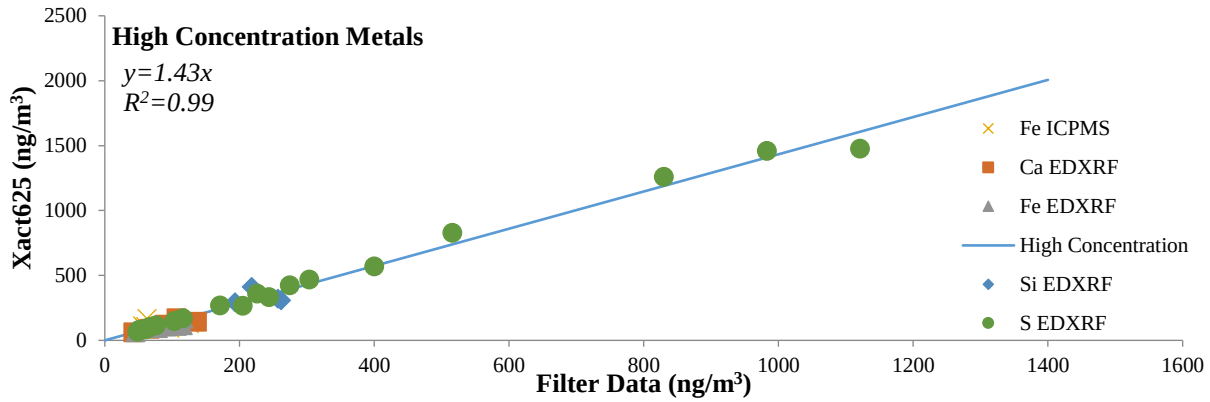

Figure S3d. Filter-Xact comparison for metals with average concentrations >50ng/m^3.

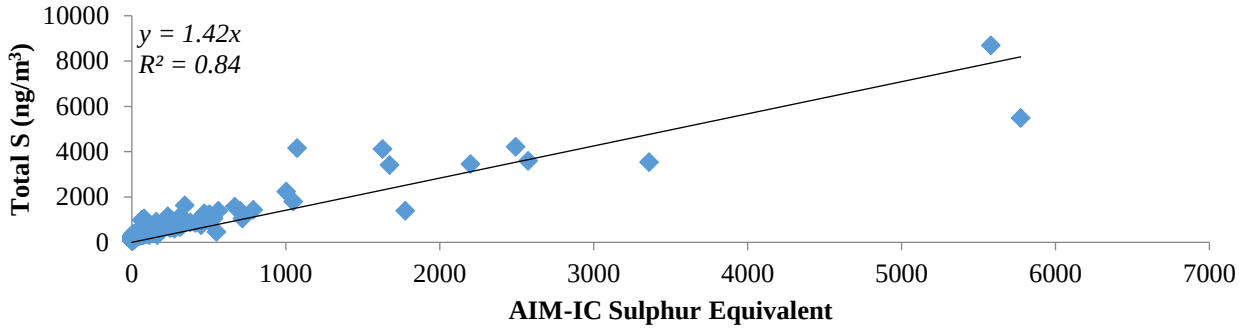

Figure S3e. AIM-IC/Xact comparison for sulphur before Aug. 25, 2013.

After the instrument was returned to the laboratory, all metal standards were run to assess the accuracy, precision, and uncertainty of each metal. High-concentration metal standards, between 7650 and 40852 ng/cm^2 in concentration, were initially run for each metal between 3 and 7 times, and each metal was found to have an accuracy and precision in the range of 98-113% and 0.3-17%, respectively (Table S1). The metal-specific analytic uncertainty was then calculated based on the sum of the average ratio of the difference between the target (T) and measured (X) values of each run (α) divided by the target value multiplied by the total number of runs (A), the uncertainty of the flow rate accuracy, set to be 10%, and additional metal-specific uncertainties (M), as seen in Equation 1. If the resulting uncertainty of any metal was less than 10%, it was raised to 10%; if there was no metal standard available for a measure metal, it was assigned an uncertainty based on the average uncertainties of the rest of the metals in the corresponding energy level. The results of this can be seen in Table S1.

$$\left\{\left|\frac{\sum_{a=1}^{A}(X-T)}{A*T}\right|^2 + 0.1^2\right\}^{1/2} + M$$ Equation 1: uncertainty calculation

Concerns that the high concentration metal standards were unrepresentative of the metal concentrations witnessed throughout the campaign led to a secondary test of 6 medium-concentration metal standards; S, V, Ba, Fe, Zn, Ni (Table S.1). These metal standards, chosen as they represented all 3 energy levels of the Xact, ranged in value from 490 ng/cm^2 to 2010 ng/cm^2, were much closer to the instrument's measurements during the campaign (between 0.1 and 1300). Based on these medium standards the metal analysis by the Xact was estimated to have accuracies in the range of 93-113% and precisions in the range of 0.2%-9.5% (Table S1), which was similar to those seen in the high concentration metal standards.

Table S1. Uncertainties, energy levels, accuracies, and precisions of the metal analysis by the Xact used for the PMF analysis of the intensive monitoring campaign.

		High Concentration Element Standards		***Medium Concentration Element Standards***		
Element	**Energy Level**	**Accuracy (measured value/target value*100%)**	**Precision (95% CI/target value*100%)**	**Accuracy (measured value/target value*100%)**	**Precision (95% CI/target value*100%)**	**Uncertainty (%)**
Si	1					14
S	1	98	12	108	9.5	12
K	1					12
Ni	2	113	17	102	0.3	18
Ca	1	108	1			16
Cd	3	99	7			10
Se	2	99	1			10
Mn	1	101	4			10
Ti	1	102	4			10
V	1	104	4	93	3.7	11
Cr	1	104	0.5			11
Fe	2	100	2	106	0.2	10
Cu	2	99	2			10
Zn	2	102	0.3	113	1.9	10
Br	2					11
Sr	2					10

Despite the variations in the slopes that the high, medium, and low concentration metals exhibited when compared to the co-measured filter samples, the r^2 values were high (over 0.95) (Figure 3). This, in addition to the results from the high and medium metal standards, led to the conclusion that the concentrations measured by the Xact were precise and largely accurate for most metals.

Unresolved divergence remained among the Xact, AIM-IC, SP-AMS, and filter measurements for some elements such as sulphur. The agreement between the medium and high concentration standards indicated that this was not due to non-linearity in the calibration.

S.2 PMF

Prior to analysis with PMF, the data for both the filter and intensive monitoring campaigns were pre-treated for Quality Control. In addition to only allowing metals which had >10% above DL data into the PMF matrices, the data matrices were also treated for biases. As the intensive monitoring campaign measured one blank value every 24 to 48 -hr, these blank values were averaged to create a single 'baseline bias' for each metal from which every datum was subtracted. This was possible as the blank values did not vary from measurement to measurement. This was not the case in the filter campaign. As the blank measurements were spaced a large temporal distance apart, and the values had wide variances, the data measured in this campaign were subtracted from the blank value which was the closest temporally.

Special consideration was given to the input data (X) and uncertainty (σ) matrices by sorting the data into three categories: above the DL, below the DL, and missing values (Xie et al., 1999). Data above the DL was input directly, with an uncertainty of σ_{ij} + DL/3. Data below the DL was replaced with DL/2, and given an uncertainty of 5(DL)/6. Missing values were replaced with the geometric mean of the measured concentrations (v), and had the highest uncertainty of the three categories (4v) (Xie et al., 1999). Additionally, each remaining metal species was classified as good, weak, or bad depending on the S/N ratio (Equation 2). Metal species with an S/N ratio above 2 were classified as good, while weak data had an S/N ratio between 0.2 and 2, and were down-weighted by a factor of 3 (Paatero and Hopke, 2003, Norris and Duvall, 2014) (Table S2). Data with an S/N ratio below 0.2 were classified as "bad" and given a weight of zero (Paatero and Hopke, 2003). The only exception to this was Cu, which had an S/N ratio of 2.76, but was classified as 'weak'. This was done as all measurements that were above the DL were very close to the DL, raising their uncertainties. Finally, the data set were all given an additional 10% "Extra Modelling Uncertainty" to further reduce the effects of noise within the data (Norris and Duvall, 2014).

$$S/N = \sqrt{\sum_{i=1}^{n} x_i^2 / \sum_{i=1}^{n} \sigma_i^2} \qquad \text{Equation 2}$$

Table S2. Minimum detection limits (DL), S/N ratios, and average values of elements measured by the Xact and analyzed using PMF.

Element	DL (ng/m^3)	S/N Ratio	Average Value (ng/m^3)
Si	107.0	3.72	143
S	26.7	8.10	468
K	11.1	4.29	31
Ca	26.2	3.89	54
Ti	1.9	4.79	3.4
V	0.3	3.22	0.21
Cr	5.1	1.82	0.04
Mn	0.4	2.40	1.12
Fe	21.8	4.78	60
Ni	0.3	0.80	0.08
Cu	1.8	2.76	2.04
Zn	1.4	0.75	0.88
Se	0.2	1.50	0.07
Br	0.2	4.79	0.54
Sr	0.9	0.82	0.23

The Q value (Equation 3) calculated by PMF algorithm was used to determine the number of resolvable factors affecting the receptor site, through its stability and inflection point. Because different pseudorandom numbers are selected by the algorithm at the initiation of each run, a stable solution with a preset number of factors will not experience a change in the Q value through a series of runs (Xie et al., 1999). Also, since the Q value of the solution decreases with an increase in the preset number of output factors, an inflection point in the rate of decrease will indicate the most central, or optimal, solution (Xie et al., 1999) (Figure S4). The optimal number of factors was also determined by examination of the G-space plot, a direct comparison of the time series (G matrix) of one factor against that of another factor, and the scaled residuals of the results. Factor solutions that contain metals with a non-normal distribution in the scaled residual could signify that the uncertainty of the metal is too low, that there is noise in the data, or that there is another pollutant source of the metal not separated in the factor solution (Paatero, 1996). It should also be noted that a linear relationship between two factors in the G-space plot could signify either a co-aligned or identical source (Paatero et al., 2005).

$$Q = \sum_{i=1}^{n} \sum_{j=1}^{m} {E_{ij}}^2 / {\sigma_{ij}}^2$$ Equation 3

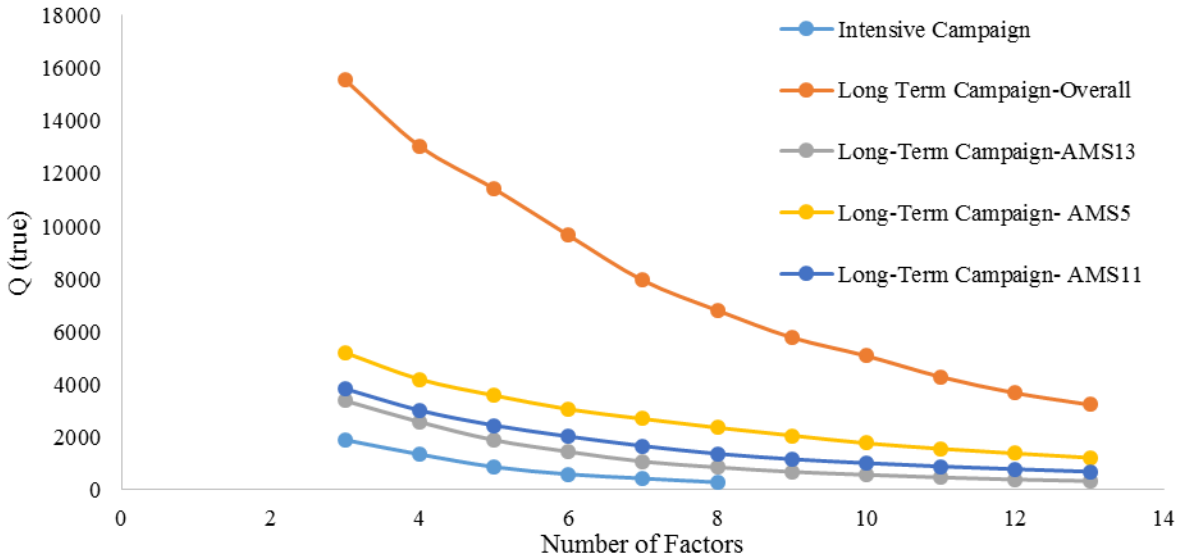

Figure S4. Q analysis of the intensive and long-term campaigns.

The final parameter examined in the selection of the optimal solution for the receptor site was the user-specified rotational parameter, Φ, chosen for the FPEAK analysis. When the PMF algorithm is run normally, i.e. with Φ=0, it finds the optimal solution the farthest away from any zeros in both the G and the F matrices (Paatero et al., 2002). When the value of Φ is changed to lie between -2 and 2, in the FPEAK analysis, the rotation of the algorithm is altered to allow for zeros or negative numbers in either the G or the F matrix. A stable solution will not change radically when the rotation, Φ, is changed, but the change in rotation may "clean" the solution by allowing the minor elements of the factor to go to zero. Throughout this study, the value of Φ was selected to be 0.

Both the filter and the Xact data were analyzed separately using PMF due to their difference in the sampling intervals. Filter data from the monitoring and the filter campaign were combined to produce a single data matrix. Additionally, the filter data from all three sites were combined into one data set prior to running the PMF algorithm. The goal of this was to take advantage of the close proximity and remote nature of the three sampling locations, assuming most, if not all

aerosol sources are common among the sites, at the expense of independent PMF solutions. The spatial variability of the sites may also add extra factor-discriminating power, as each site is in a different direction to the various sources. This technique succeeded in producing a stable 5-factor solution, which was similar to the 5-factor solutions produced when the filter data from each site was run independently (AMS 5, AMS 11, and AMS 13). Not only did the 5-factor solution exhibit the most central and stable Q factor, but also proved to be the most physically meaningful when compared to the solutions with 6 and 7 factors (Supplementary S.3). Overall, combining the three data sets stabilized the Q factor of the input data, as can be seen from the clear lowest standard deviation in the Long-term Campaign- Combined filters versus the individual sites' standard deviations (Table S3).

Table S3. Standard deviations of the Q-factor across 150 PMF runs for the intensive monitoring and long-term campaigns.

Number of Factors	Intensive Monitoring Campaign	Long-term Campaign-Combined Filters	Long-term Campaign AMS13	Long-term Campaign-AMS5	Long-term Campaign-AMS11
3	0.3	270	93	0.02	71
4	22	31	52	110	0.2
5	0.4	27	18	6.8	0.1
6	0.5	41	14	24	15
7	1.9	150	5.5	13	31
8	11	57	5.5	27	32
9		160	5.6	21	8.7
10		100	5.4	47	11
11		36	5.2	48	11
12		100	5.3	32	9.6
13		19	5.3	26	

In order to determine the relative weights of the different factors, a multiple linear regression of the time series of each factor for both campaigns was run against both the summed metal concentrations as well as the $PM_{2.5}$ concentrations (obtained from WBEA). As trace metals only account for a small percentage of the overall $PM_{2.5}$ mass, the results of the $PM_{2.5}$ regression proved to be a poor fit both statistically ($r^2<0.8$) and physically, as it resulted in negative relative weights, to the metal speciation factor solutions. Because of this, the total metals concentration was used to determine the relative weights of the different factors, which resulted in a much better fit ($r^2>0.99$).

S.3 PMF Factor Solutions

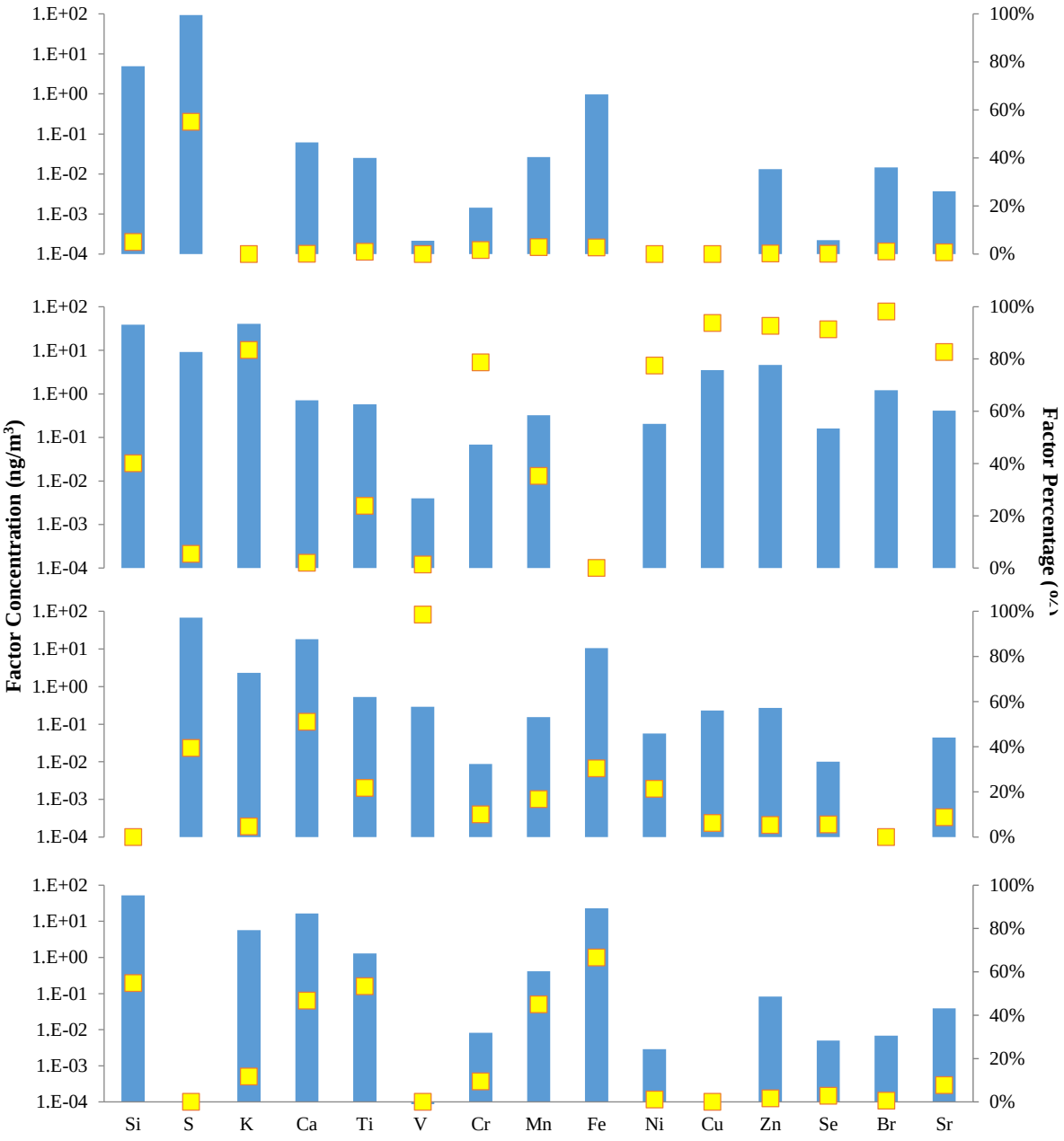

Figure S5. Alternative 4-factor solution calculated using PMF for the intensive campaign (Xact metal data).

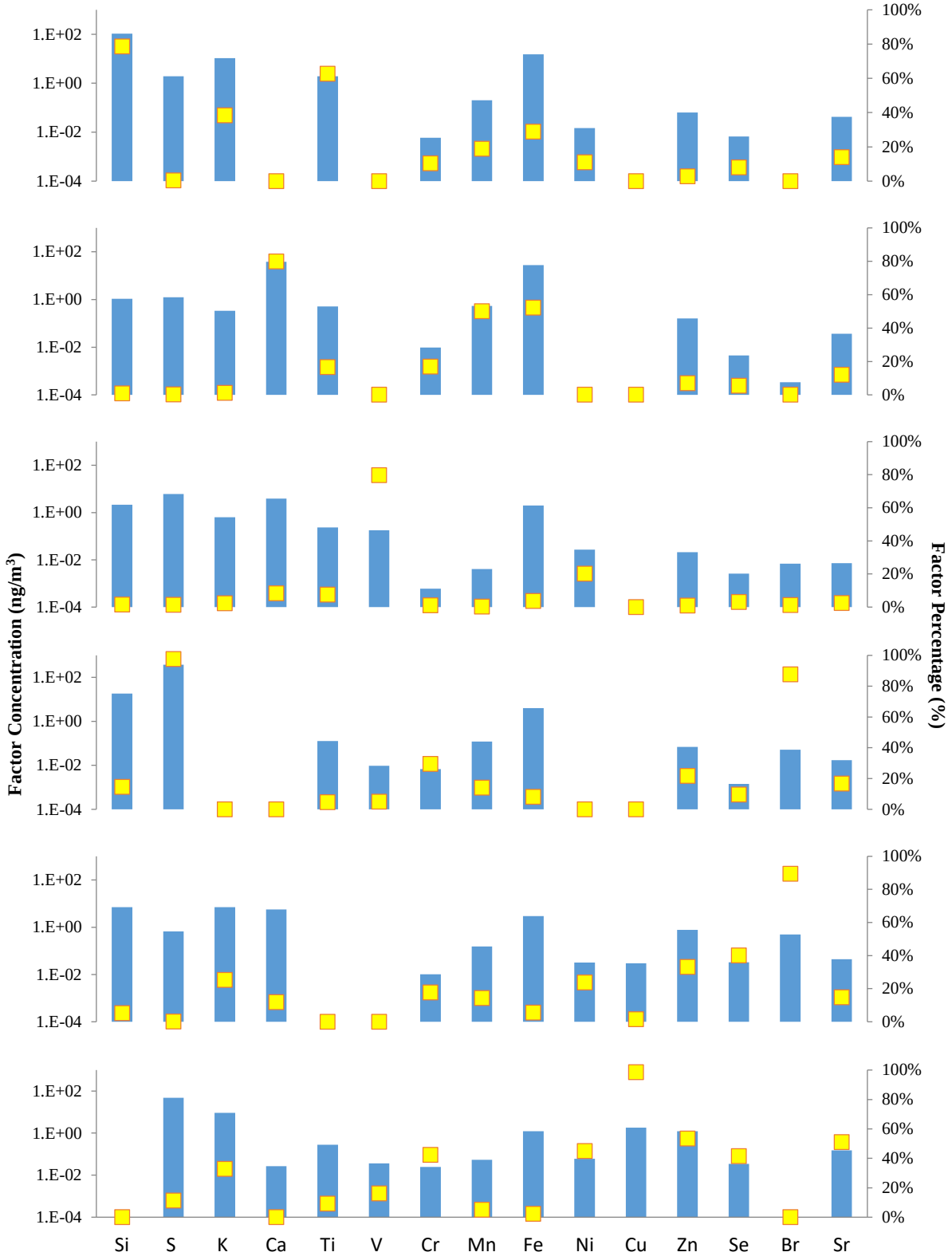

Figure S6. Alternative 6-factor solution calculated using PMF for the intensive campaign (Xact metal data).

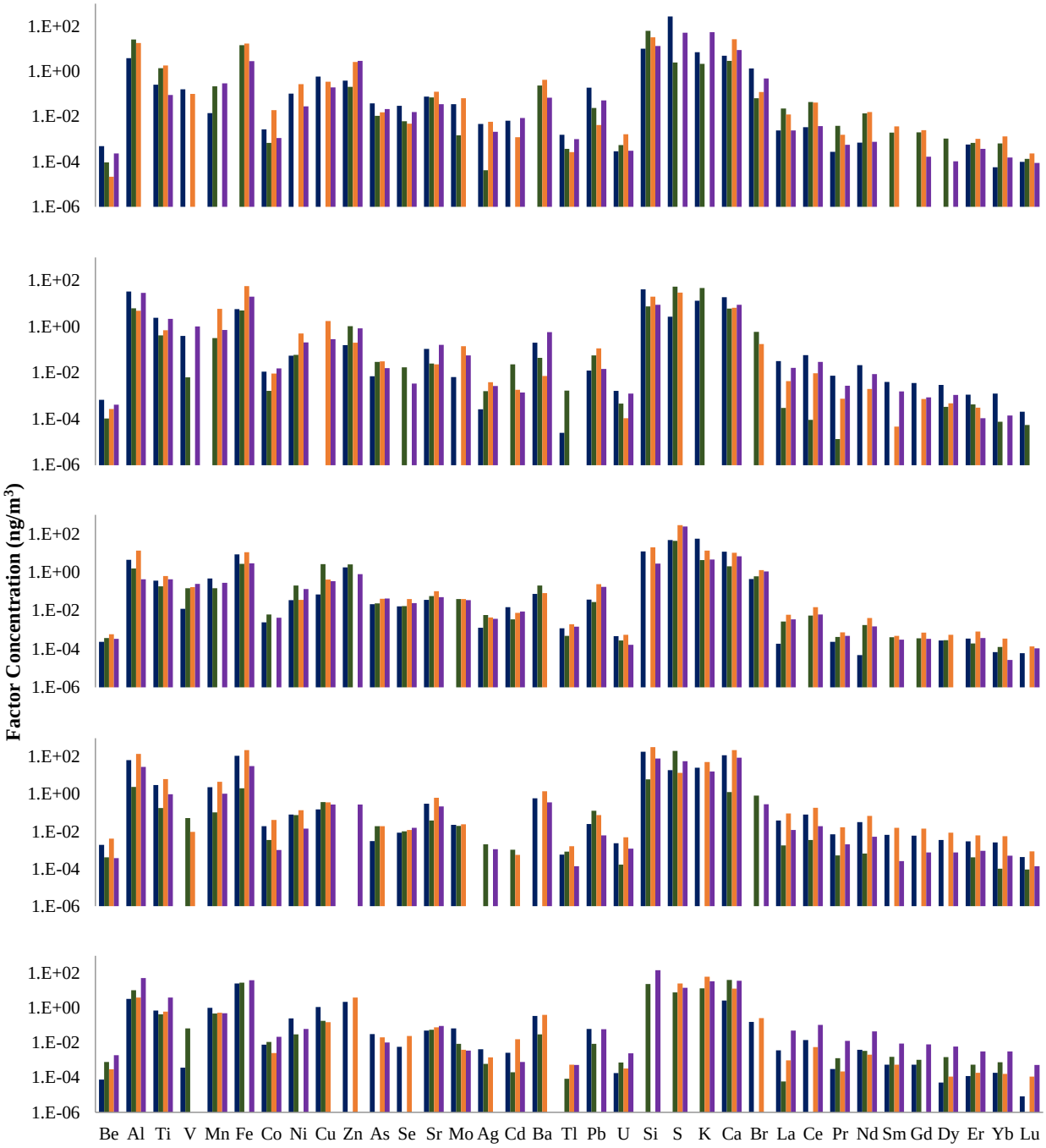

Figure S7. 5-factor solutions for 4 independently run PMF analyses of the long-term campaign data (Integrated filter data). Dark blue is the overall solution run after combining the data from all three sites; green is the independently run AMS13 data; orange is the independently run AMS5 data; and purple is the independently run AMS11 data.

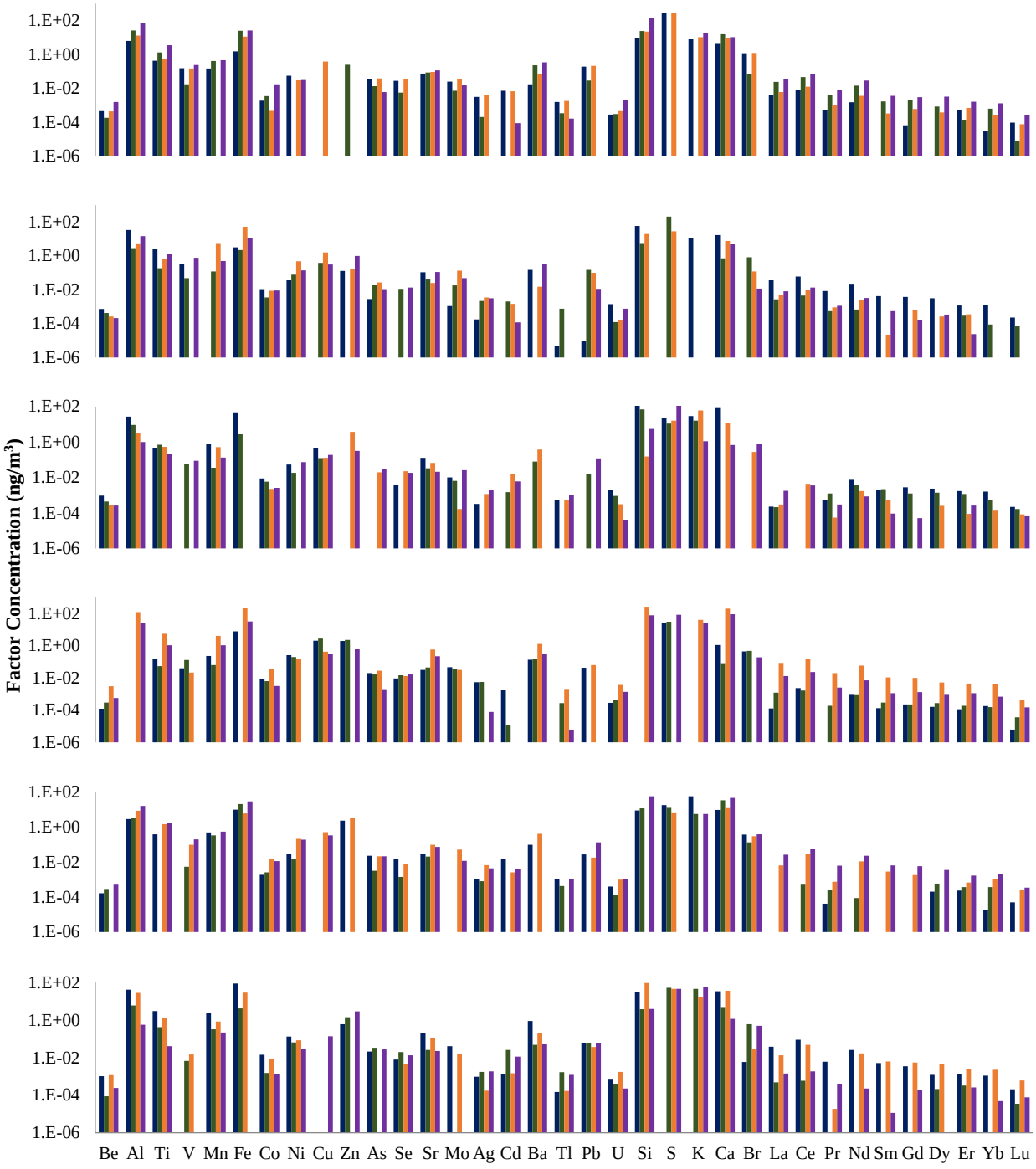

Figure S8. 6-factor solutions for 4 independently run PMF analyses of the long-term campaign data (Integrated filter data). Dark blue is the overall solution run after combining the data from all three sites; green is the independently run AMS13 data; orange is the independently run AMS5 data; and purple is the independently run AMS11 data.

S.4 Overall Species comparison

Table S4. Average concentrations of elements used in the PMF analysis of the long-term campaign average and 90th percentile (Dec. 2010-Nov. 2012, Aug. 2013) for all three sites compared to average metal concentrations in Halifax, St John, Montreal, Windsor, Toronto, Edmonton, and Vancouver (Environment Canada, 2015). All metal(oid)s are measured either by acid digested ICP-MS ([1]) or ED-XRF ([2]).

Element (ng/m³)	Oil Sands - Average	Oil Sands- 90th Percentile	Halifax, NS	St John, NB	Montreal, QC	Windsor, ON	Toronto, ON	Edmonton, AB	Vancouver, BC
***Ag*[1]**	0.02	0.02	0.02	0.02	0.04	0.03	0.03	0.03	0.03
***Al*[2]**	**121**	**290**	36	31	43	29	31	47	29
***As*[1]**	0.12	0.25	0.25	0.25	0.83	1.0	0.48	0.41	0.51
***Ba*[1]**	1.4	**3.5**	1.2	0.88	1.79	2.26	2.45	2.87	2.42
***Be*[1]**	N/A	N/A	0.005	0.004	0.005	0.005	0.004	0.005	0.004
***Br*[2]**	2.1	**4.3**	2.0	1.8	2.5	2.7	2.0	2.6	2.0
***Ca*[2]**	**154**	**390**	23	14	58	69	45	60	19
***Cd*[1]**	0.04	0.08	0.03	0.04	0.19	0.16	0.08	0.13	0.07
***Ce*[1]**	0.16	0.35							
***Co*[1]**	0.05	0.11	0.12	0.02	0.03	0.02	0.03	0.15	0.03
***Cr*[1]**	N/A	N/A	0.23	0.21	0.54	0.43	0.37	1.6	0.55
***Cu*[1]**	2.7	**6.0**	2.0	1.2	3.2	3.3	2.8	3.6	2.7
***Dy*[1]**	0.01	0.02							
***Er*[1]**	0.01	0.02							
***Fe*[2]**	**151**	**350**	32	20	59	123	51	120	52
***Gd*[1]**	0.01	0.03							
***K*[2]**	**97**	**200**	51	42	75	70	48	66	56
***La*[1]**	0.08	0.17							
***Lu*[1]**	N/A	L/A							
***Mn*[1]**	5.1	**13**	0.91	0.60	2.2	4.5	1.6	7.7	2.6
***Mo*[1]**	0.21	0.39	0.11	0.09	0.31	0.33	0.18	0.40	0.22
***Ni*[1]**	0.94	1.4	**2.3**	0.76	0.73	0.75	0.46	**1.5**	**1.4**
***Nd*[1]**	0.06	0.14							
***Pb*[1]**	0.42	0.99	1.5	0.85	3.9	4.3	2.0	1.4	2.5
***Pr*[1]**	0.02	0.04							
***S*[2]**	373	**760**	334	357	415	**720**	455	331	248
***Se*[1]**	0.09	0.15	0.19	0.20	0.63	1.1	0.57	015	0.15
***Si*[2]**	**265**	**670**	46	29	54	53	40	14	26
***Sm*[1]**	0.01	0.03							
***Sr*[1]**	N/A	N/A	0.50	0.48	0.69	0.78	0.58	0.50	0.62
***Ti*[1]**	**7.3**	**15**	0.85	0.32	1.6	0.52	0.35	0.61	0.38
***Tl*[1]**	0.01	0.03	0.02	0.02	0.02	0.03	0.02	0.01	0.01
***U*[1]**	N/A	N/A							
***V*[1]**	0.84	1.9	**2.9**	1.2	0.81	0.71	0.23	0.35	**2.4**
***Yb*[1]**	N/A	N/A							
***Zn*[1]**	6.4	14	6.5	8.6	16	**22**	10	12	8.9

S.5 Shannon Entropy

Shannon entropy is a theoretical measure of the uncertainty associated with a random variable (Healy et al., 2014). Shannon entropy was used to quantify how each species was partitioned across various factors. The bulk population diversity (D_i) for each species (i) was determined based on the mass fractions of each species (p^a) for each factor (a) across the total number of factors (A). A species equally distributed across all five factors would have a diversity of 5: a species with a value of 1 is considered to be entirely distributed to a single factor. Overall, Shannon Entropy is an information-theoretic measure that has been previously used to indicate biodiversity (Whittaker, 1965), genetic diversity (Rosenburg et al., 2002), and economic diversity (Attaran, 1986). More recently, Shannon entropy has been used to analyze how chemical species present in particles are distributed in an aerosol population (Healy et al., 2014; Reimer and West, 2013). In this study, Shannon entropy was used to analyze how the metals species were distributed across the various factors. A metal species with a diversity value above 3.5 was considered to be equally distributed, and, therefore, that species could not be used as a characteristic species for factor identification.

$$D_i = e^{\sum_{a=1}^{A} -p^a ln p^a} \qquad \text{Equation 4}$$

Table S4. Diversity values for the elements analyzed in the intensive monitoring and long-term campaigns. Species in bold had diversity values greater than 3.5 and thus were too diverse to be used to distinguish between factors.

Elements	Intensive Campaign	Long-term Campaign
Si	2.0	2.4
S	2.1	1.8
K	2.4	3.3
Ca	2.3	2.2
Ti	2.6	3.3
V	1.6	2.4
Cr	**3.9**	
Mn	3.5	2.3
Fe	3.1	2.1
Ni	2.6	**3.7**
Cu	1.4	1.9
Zn	2.0	2.8
Se	2.2	3.6
Br	1.5	2.6
Sr	3. 5	**3.6**
Be		**3.5**
Al		2.6
Co		**3.8**
As		**4.2**
Mo		2.9
Ag		3.4
Cd		2.2
Ce		2.6
Ba		2.8
La		2.6
Pr		2.4
Nd		2.5
Sm		2.2
Gd		2.3
Dy		2.4
Er		3.2
Yb		2.4
Lu		3.2
Tl		3.0
Pb		3.4
U		3.4

S.6 Temporal trends

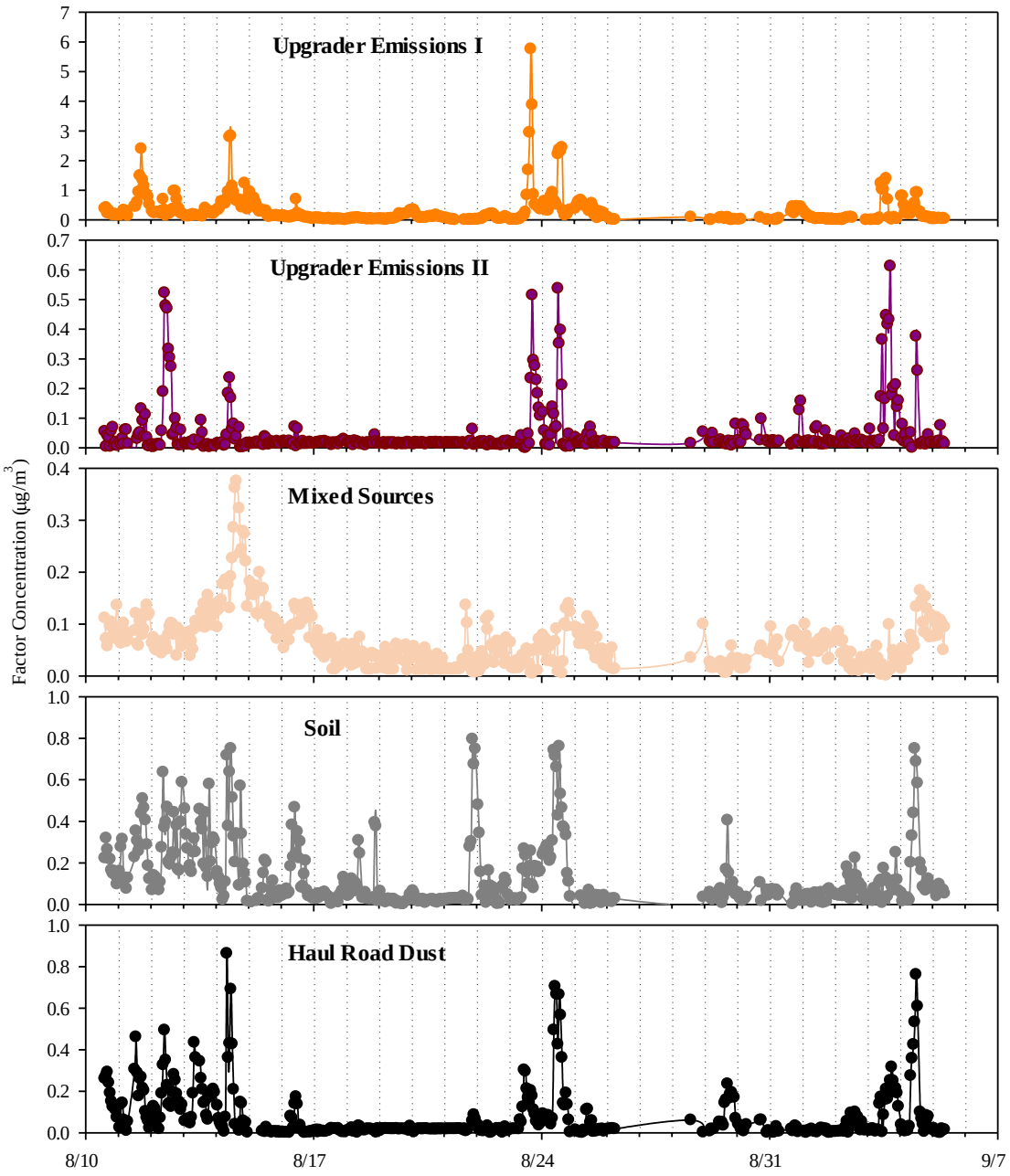

Figure S10. Concentration time series of PMF-resolved 5 factor during the intensive campaign.

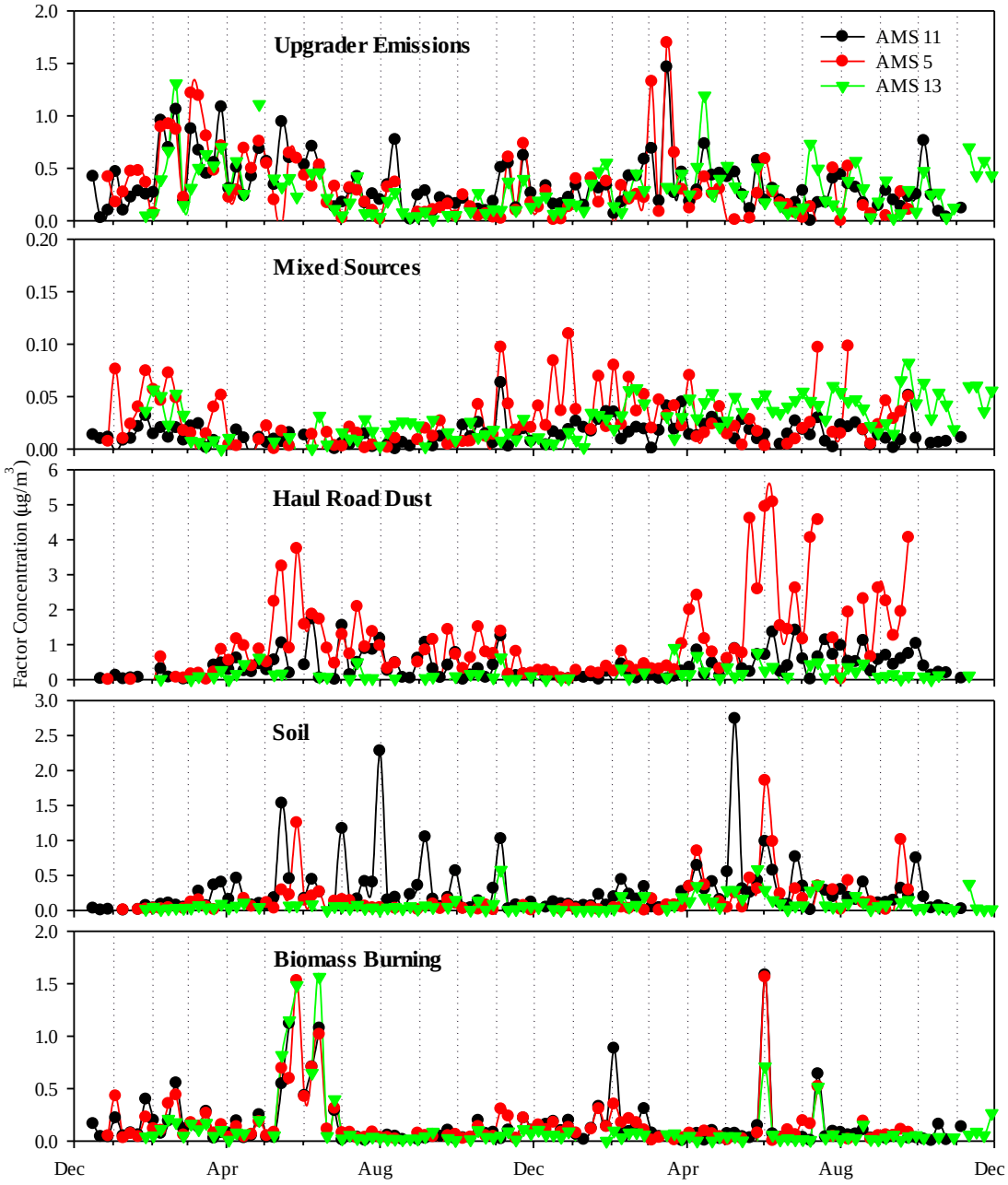

Figure 11. Concentration time series of PMF-resolved 5 factors during the long-term campaign from December, 2010 to November, 2012 for AMS13, AMS5, and AMS11.

S.7 Seasonal and Geographical Wind Directions

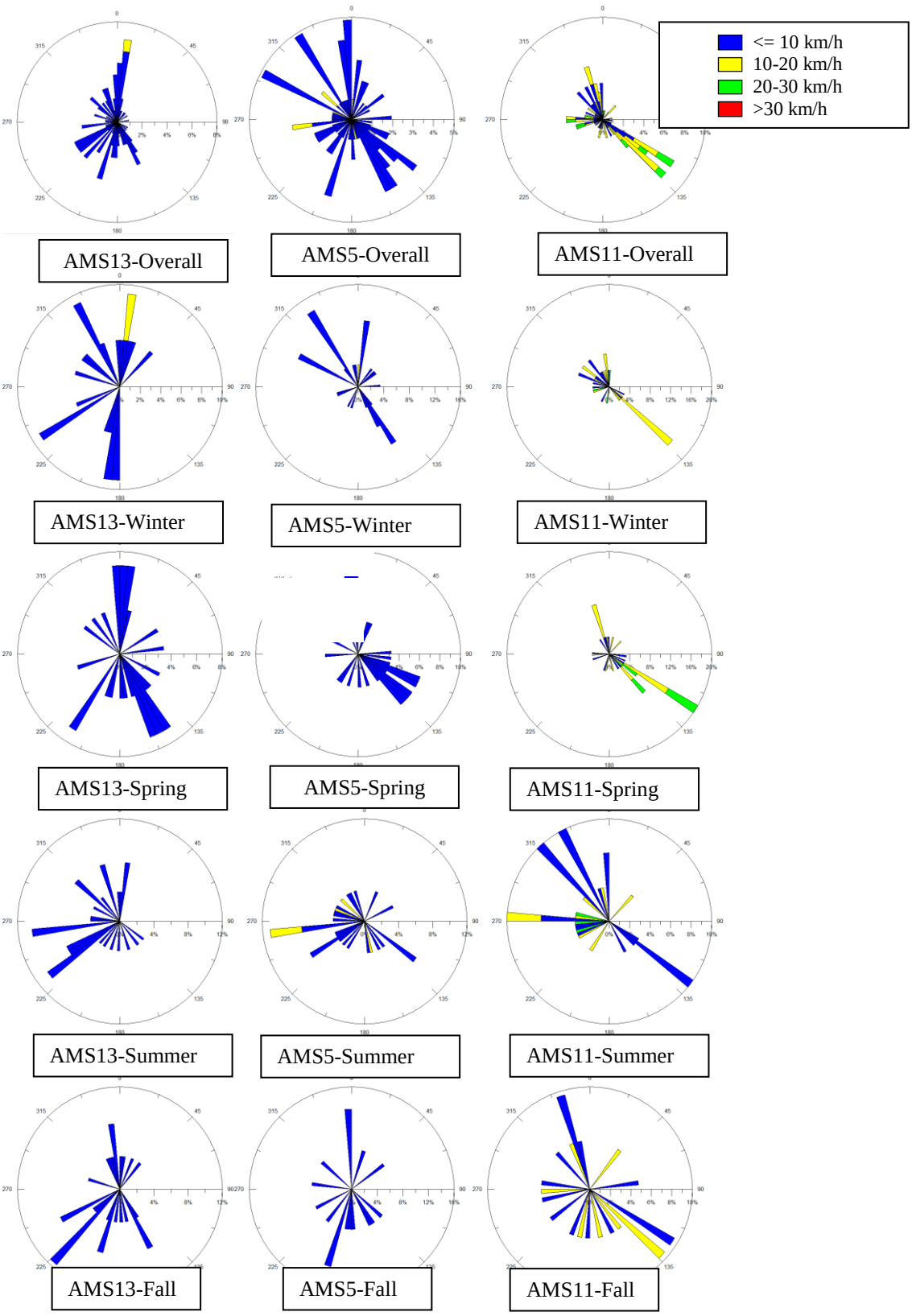

Figure S12. Overall and seasonal wind roses of the three sites analyzed in the long-term campaign.

S.8 Seasonal Temperatures

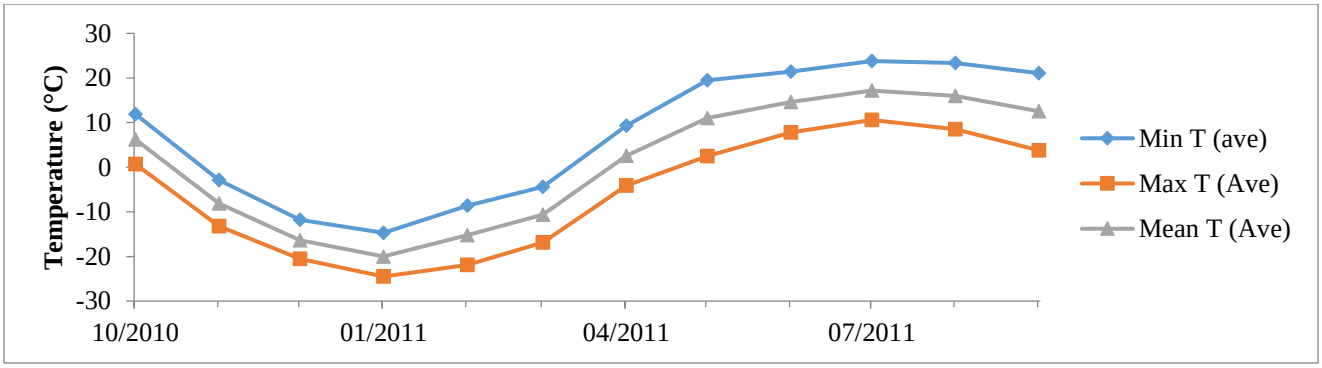

Figure S13. Typical average monthly temperatures for Fort McMurray, AB for the year 2010-2011.

S.9 Long-Term Campaign CPF Plots

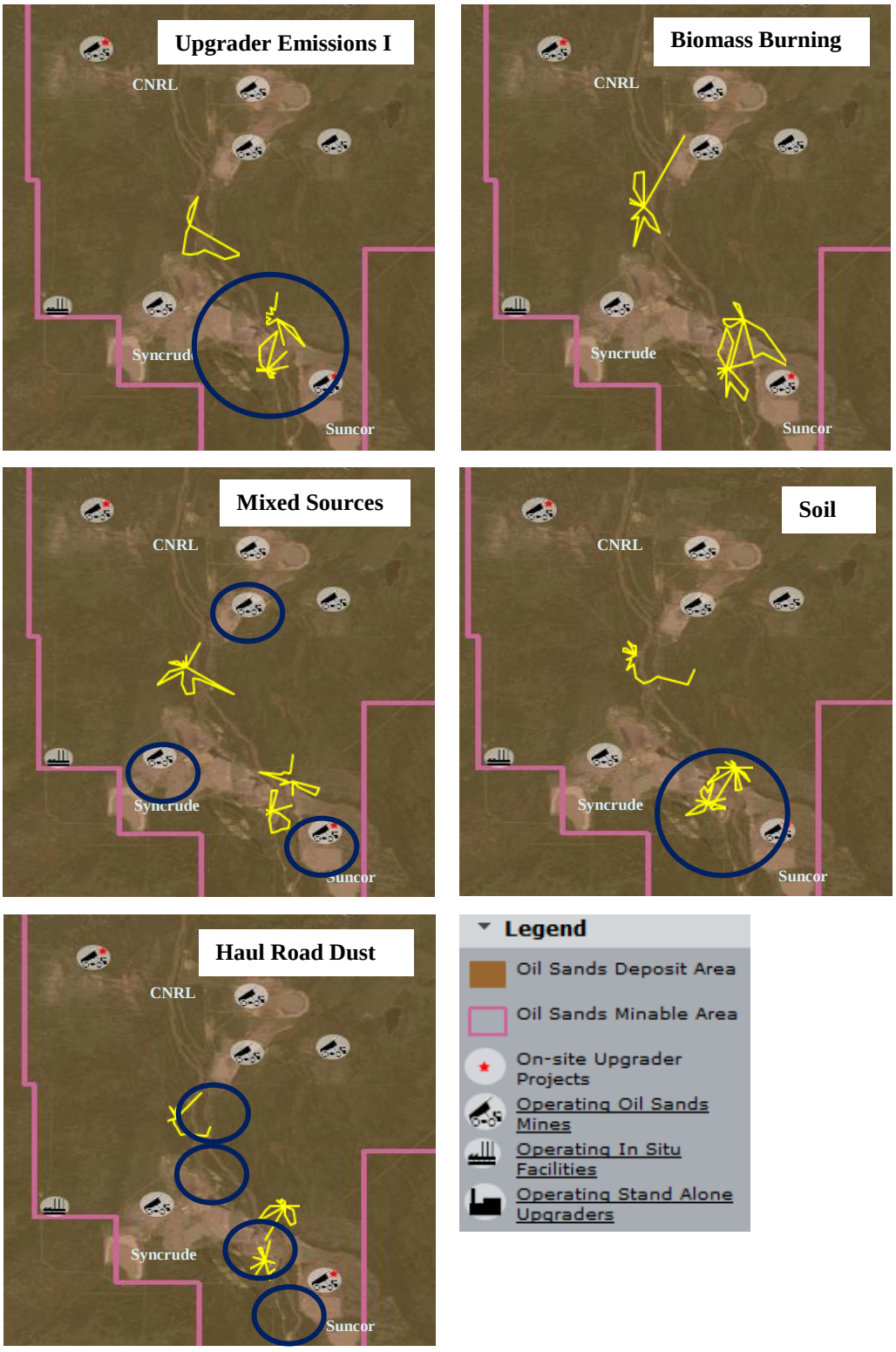

Figure S14. CPF plots from all three sites; AMS13, AMS5, and AMS11 for each factor identified using PMF on the long-term campaign's data. Blue Circles indicate the location of potential sources. 'Gaps' in the yellow wind rose are due to a lack of wind data coming from certain directions. ***Map courtesy of Alberta: Environmental and Sustainable Resource Development. Available: http://osip.alberta.ca/map***

S.10 HYSPLIT Analysis

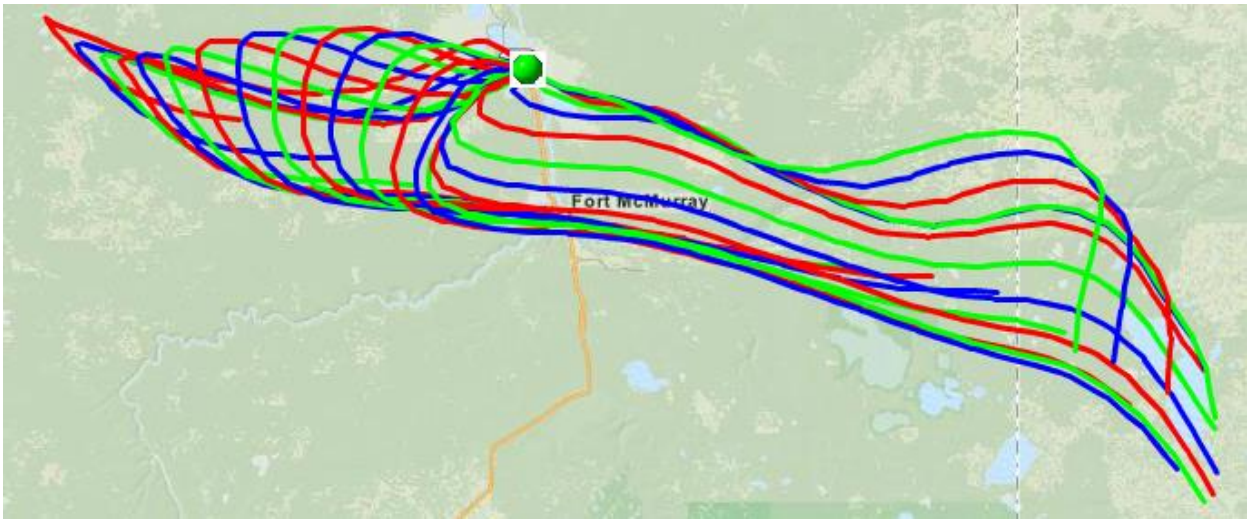

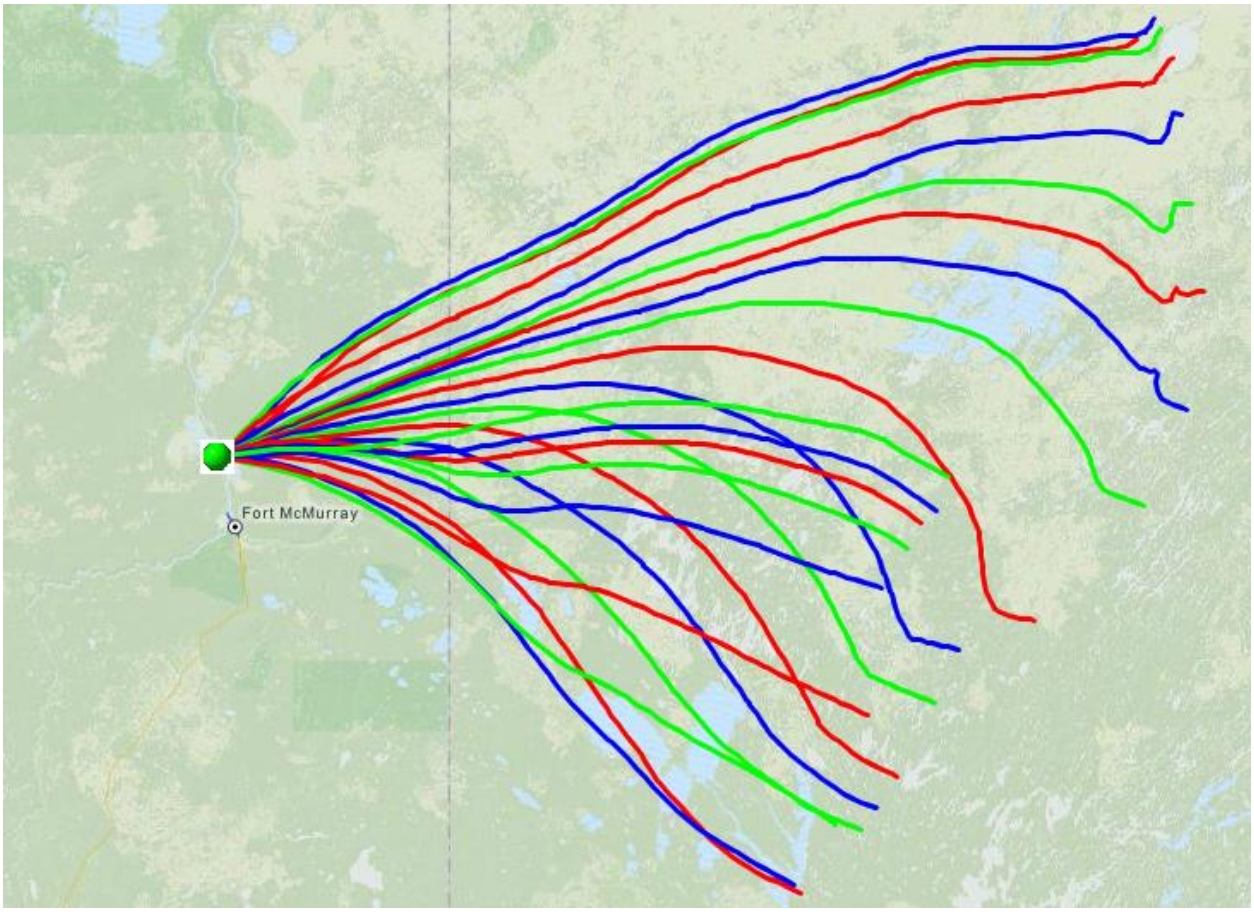

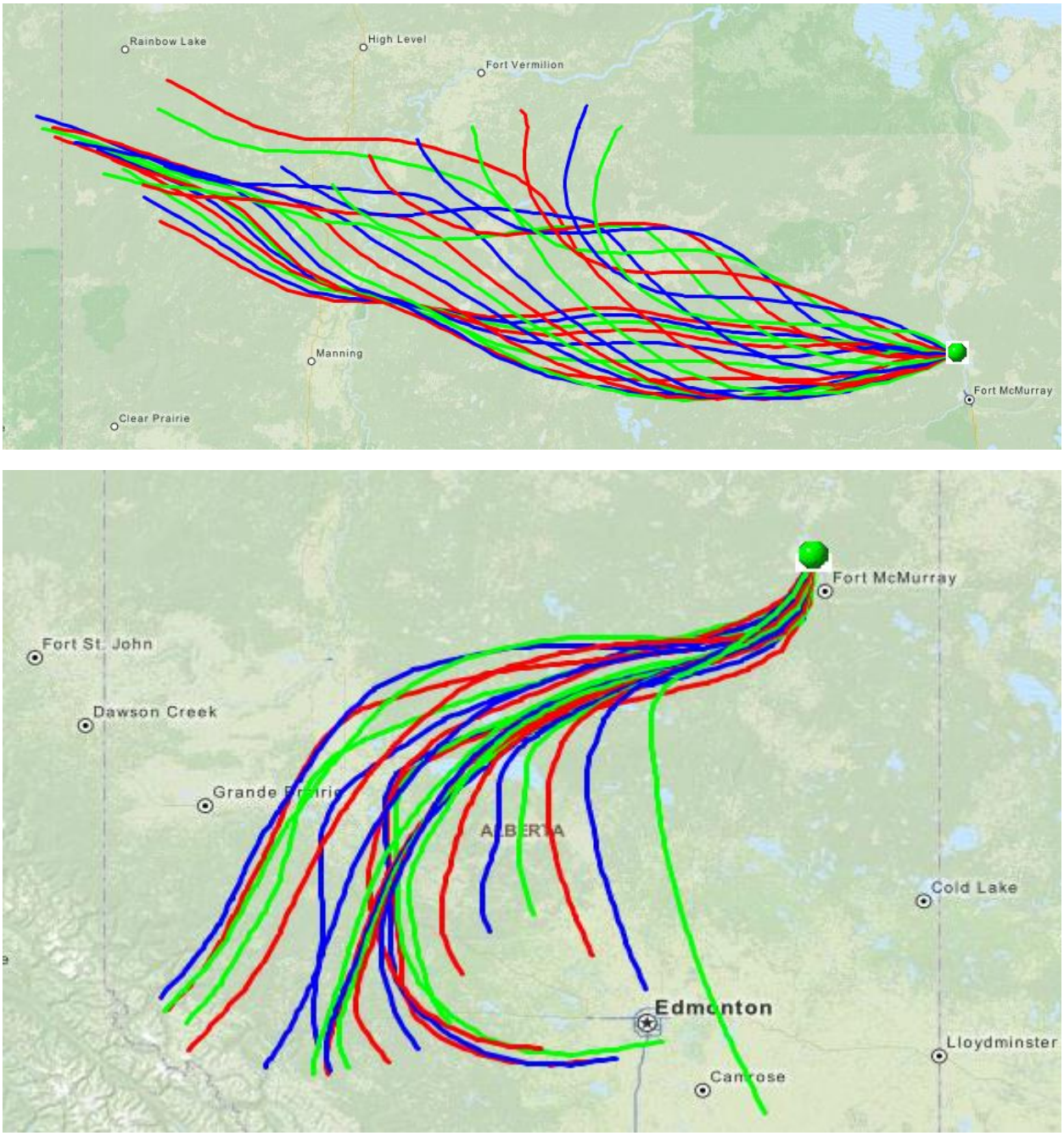

Figure S15. HYSPLIT Analysis diagrams of the 4 days with the overall highest contributions of the biomass burning factor: June 2, 2011; June 14, 2011; May 27, 2011; May 21, 2011.

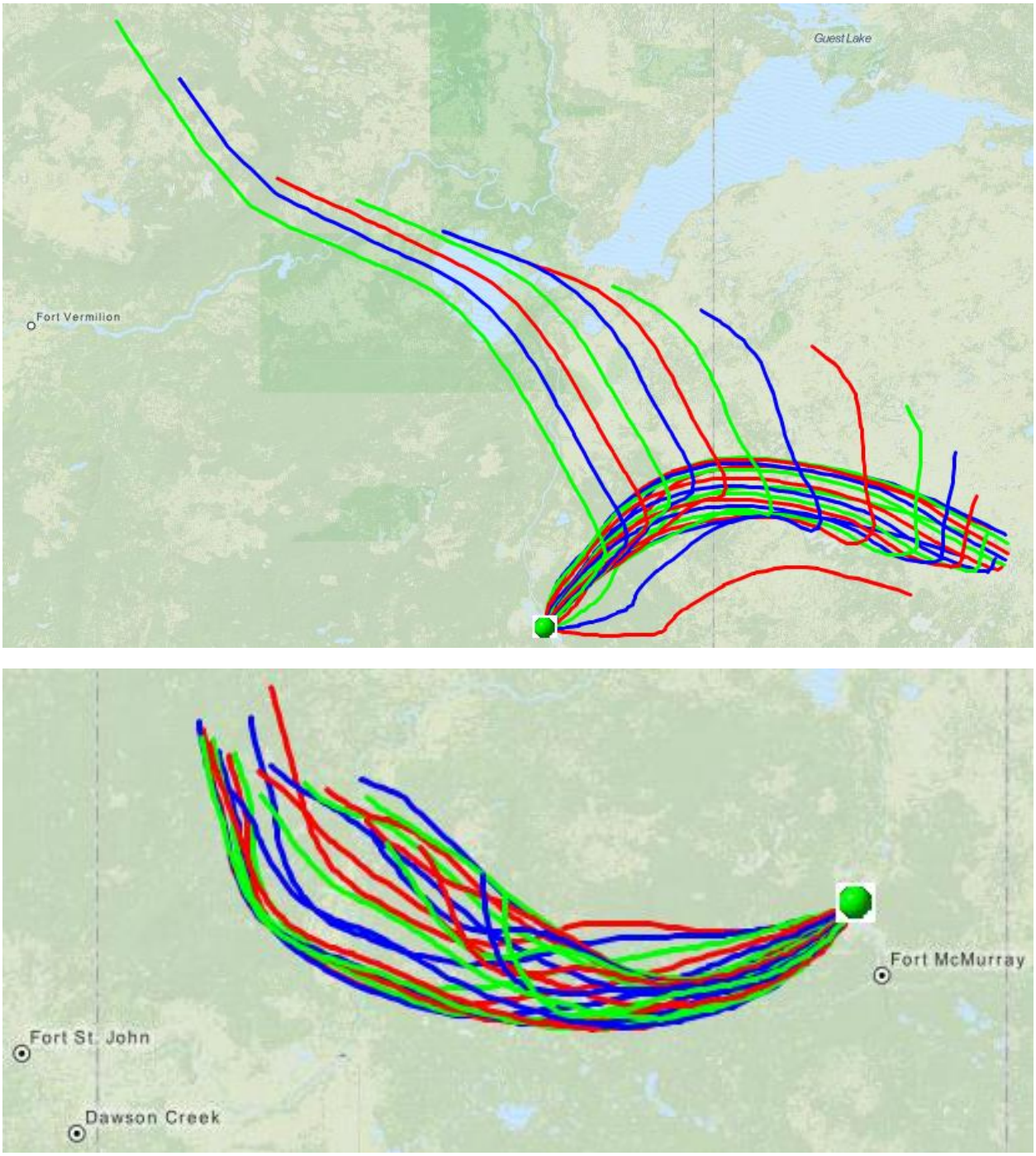

Figure S16. HYSPLIT analysis diagrams of the 2 days with the highest overall soil contributions: June 8, 2011; March 22, 2012.

References

Attaran, M.: Industrial diversity and economic performance in U.S. areas, Ann. Regional Sci., 20, 44-54, 1986.

Environmental Technology Verification Report: Cooper Environmental Services LLC Xact 625 Particulate Metals Monitor, Portland, OR, USEPA, 2012

Environment Canada, NAPS Data Products, http://maps-cartes.ec.gc.ca/rnspa-naps/data.aspx, last access Jan. 2015.

Government of Canada, 2010-2011 Climate, http://climate.weather.gc.ca/climateData/dailydata_e.html?timeframe=2&Prov=AB&StationID=31288&dlyRange=2008-07-03|2011-10-20&cmdB2=Go&cmdB1=Go&Year=2010&Month=11&Day=5, last access Jan. 3, 2015.

Healy, R. M., Riemer, N., Wenger, J. C., Murphy, M., West, M., Poulain, L., Wiedensohler, A., O'Connor, I. P., McGillicuddy, E., Sodeau, J. R., and Evans, G. J.: Single particle diversity and mixing state measurements, Atmos. Chem. Phys., 14, 6289-6299, doi:10.5194/acp-14-6289-2014, 2014.

Markovic, M. Z., VandenBoer, T. C., and Murphy, J. G.: Characterization and optimization of an online system for the simultaneous measurement of atmospheric water-soluble constituents in the gas and particle phases, J. Environ. Monitor., 14, 1872-1884, 2012.

Norris, G. and Duvall, R.: EPA Positive Matrix Factorization (PMF) 5.0: Fundamentals and User Guide, Petaluma, CA, United States of America Environmental Protection Agency, 2014.

Paatero, P.: User's Guide for Positive Matrix Factorization Programs, PMF2.EXE and PMF3.EXE. Helsinki: University of Helsinki, 1996.

Paatero, P. and Hopke, P.: Utilizing wind direction and wind speed as independent variables in multilinear receptor modeling studies, Chemometr. Intell. Lab., 60, 25-41, 2002.

Paatero, P. and Hopke, P.: Discarding of downweighting high-noise variables in factor analytic models, Anal. Chim. Acta, 490, 277-289, 2003.

Paatero, P., Hopke, P., Begum, B., and Biswas, S.: A graphical diagnostic method for assessing the rotation in factor analytical models of atmospheric pollution, Atmos. Environ., 39, 193-201, 2005.

Paatero, P., Hopke, P., Song, X.-H., and Ramadan, Z.: Understanding and controlling rotations in factor analytic models, Chemometr. Intell. Lab, 60, 253-264, 2002.

Reimer, N. and West, M.: Quantifying aerosol mixing state with entropy and diversity measures, Atmos. Chem. Phys., 13, 11423-11439, 2013.

Rosenberg, N. A., Pritchard, J. K., Weber, J. L., Cann, H. M., Kidd, K. K., Zhivotovsky, L. A., and Feldman, M. W.: Genetic structure of human populations, Science, 298, 2381-2385, 2002.

Whittaker, R.: Dominance and diversity in land plant communities: numerical relations of species express the importance of competition in community function and evolution, Science, 137, 250-260, 1965.

Willis, M. D., Lee, A. K. Y., Onasch, T. B., Fortner, E. C., Williams, L. R., Lambe, A. T., Worsnop, D. R., and Abbatt, J. P. D.: Collection efficiency of the soot-particle aerosol mass spectrometer (SP-AMS) for internally mixed particulate black carbon, Atmos. Meas. Tech., 7, 4507-4516, doi:10.5194/amt-7-4507-2014, 2014.

Xie, Y.-L., Hopke, P. K., Paatero, P., Barrie, L. A., and Li, S.-M.: Identification of source nature and seasonal variations of arctic aerosol by the Multilinear Engine, Atmos. Environ., 33, 2549-2562, 1999.